

# An Expanding Shell and Synchrotron Jet in RS Ophiuchi

Michael P. Rupen and Amy J. Mioduszewski

*National Radio Astronomy Observatory, 1003 Lopezville Road, Socorro, NM 87801*

mrupen@nrao.edu, amiodusz@nrao.edu

and

Jennifer L. Sokoloski<sup>1</sup>

*Columbia Astrophysics Laboratory, 550 W. 220th Street, 1027 Pupin Hall, Columbia University, New York, NY 10027*

jeno@astro.columbia.edu

## ABSTRACT

We report high-resolution radio imaging of the recurrent nova RS Ophiuchi (RS Oph) during the first month of the 2006 outburst, using the Very Long Baseline Array (VLBA). Observations made on days 20.8 and 26.8 of the outburst show a synchrotron-emitting partial shell that is much brighter to the east than to the west. Assuming the broad component of the infrared lines corresponds to the outermost part of the shell seen by the VLBA, the distance to the source is  $2.45 \pm 0.4$  kpc. The circular shape and spectral indices of the shell emission challenge simple models for the radio structure immediately after the outburst. The second epoch also shows an additional, resolved, synchrotron-emitting component well to the east of the shell. Its inferred velocity is comparable to the escape speed from the surface of a high-mass white dwarf. This component was not seen in the first epoch. Its appearance may be related to the outflow reaching the edge of the nebula created by the red giant wind, which had been re-filling the void left by the last outburst in 1985. This eastern component is likely related to the jets previously seen in this and other symbiotic stars, and represents the earliest clear detection of such a jet, as well as the best case yet for synchrotron emission from a white dwarf jet.

*Subject headings:* binaries: symbiotic — novae, cataclysmic variables — stars: individual (RS Oph) — stars: winds, outflows — radio continuum: stars

---

<sup>1</sup>National Science Foundation (NSF) Astronomy and Astrophysics Fellow.

## 1. Introduction

The most recent major outburst of the symbiotic star and recurrent nova RS Ophiuchi (RS Oph) was discovered near the optical peak on 2006 February 12.83 (Narumi et al. 2006), hereafter taken as time zero. RS Oph is a binary system in which a red giant deposits material through its wind onto a white dwarf (WD) companion (see, e.g., Kenyon 1986). Approximately every 20 years, the system erupts as a nova, as ‘runaway’ thermonuclear burning in the hydrogen-rich white-dwarf envelope leads to a visual brightness increase of more than 6 mag in less than 2 days, a sustained period with WD luminosity near the Eddington limit, and the ejection of material from the WD surface (e.g., Bode 1987). The last such eruption was in 1985. The frequency of these outbursts suggests that the mass of the WD in RS Oph is very close to the Chandrasekhar limit (e.g., Hachisu & Kato 2001; Sokoloski et al. 2006), making this a prime candidate for a Type Ia supernova progenitor system.

Whereas most novae detected in the radio emit via thermal free-free bremsstrahlung from the shell of ejecta (e.g., Seaquist 1989), post-outburst radio emission from RS Oph instead emanates primarily from the dense circumstellar material (CSM) that is swept up and shocked by the fairly low-mass ejected shell. Observations after the previous outburst in 1985 with the European Very Long Baseline Interferometry Network (EVN), the Multi-Element Radio Linked Interferometer Network (MERLIN), and the Very Large Array (VLA) suggested that the radio emission was initially non-thermal at low frequencies, with a possible thermal component becoming dominant later in the outburst. The radio source consisted of a resolved central component plus possible bi-polar jets expanding at 1.5 mas/day (Padin, Davis, & Bode 1985; Hjellming et al. 1986; Taylor et al. 1989; Davis 1987; Porcas, Davis, & Graham 1987).

Although jets have been observed from an increasing number of accreting white dwarfs in symbiotic stars and supersoft X-ray sources (Sokoloski et al. 2004), and even several novae (Kawabata et al. 2006; Iijima & Essenoglu 2003), these jets are generally not spatially well resolved, and basic questions such as the relationship between jet production and outbursts remain. Most jets from white dwarfs have velocities of hundreds to thousands of  $\text{km s}^{-1}$ , and when jet emission can be spatially isolated, it usually appears to be thermal (e.g., Hollis et al. 1997; Kellogg et al. 2001; Brocksopp et al. 2004; Galloway & Sokoloski 2004). In a few cases, however, observations have hinted that particles can be accelerated sufficiently that non-thermal radio and/or X-ray emission can also be produced (Crocker et al. 2001; Nichols et al. 2007).

Here we report the detection of an expanding, synchrotron-emitting ring just weeks after the nova explosion, and, between three and four weeks after the outburst, the appearance

of a synchrotron-emitting feature to the east of this ring aligned with the putative jet from 1985. We describe our observations of the expanding ring and the eastern component in §2. We discuss these observations in more detail in §3, and summarize our conclusions in §4.

## 2. Observations

We observed RS Oph with the National Radio Astronomy Observatory’s<sup>1</sup> (NRAO’s) Very Long Baseline Array (VLBA) under project code BS167 in two four-hour runs, on 2006 March 5 and 2006 March 11, corresponding to days 20.8 and 26.8 of the outburst, respectively. The first run used all antennas but Hancock, while the second used the entire 10-antenna array. We observed the source in two frequency bands, consisting of 64 MHz in each of the two dual polarizations, centered on 1.6675 and 4.9875 GHz, recorded at a rate of 256 megabits per second. To remove atmospheric and instrumental effects, we employed phase referencing using the nearby calibrators J1745–0753 (1°67 away; primary calibrator at 5.0 GHz) and J1743–0305 (3°27 away; primary calibrator at 1.7 GHz). The position of the former was taken from the Second VLBA Calibrator Survey (Fomalont et al. 2003), with a quoted (rms) accuracy of 0.50 milliarcseconds; the position of the latter was taken from the International Celestial Reference Frame (ICRF; Fey et al. 2004), with a quoted accuracy of 0.77 milliarcseconds. We correlated all four polarization pairs using the VLBA correlator in Socorro, NM, and calibrated, imaged, and self-calibrated the data in the standard fashion using NRAO’s Astronomical Image Processing System (AIPS; Greisen 2003). Phase referencing aligned the 5.0 GHz images to better than 0.5 mas. The 1.7 GHz images differed by  $\sim 8$  mas, rather larger than expected from residual ionospheric effects, but not alarmingly so, given the poor weather during the first observations. We shifted the lower frequency images to align the centers of the rings with those seen at 5.0 GHz.

Figure 1 shows the total intensity images. To a limit of a few percent (or the rms noise, whichever was higher), no linear or circular polarization was detected in either epoch, at either frequency. There may be some missing radio emission on scales much larger than sampled by the VLBA – the corrected 5 GHz flux density on day 20.8 ( $\sim 32$  mJy; see below) is somewhat lower than that seen by MERLIN at 6 GHz on the same day (about 40 mJy; O’Brien et al. 2006a).

---

<sup>1</sup>The National Radio Astronomy Observatory is a facility of the National Science Foundation operated under cooperative agreement by Associated Universities, Inc.

## 2.1. The Expanding Ring

All four images are dominated by a ring which is much brighter to the east than to the west. Despite this brightness asymmetry, the ring is consistent with being circular (Fig. 2). In particular, a two-dimensional ring with an inclination corresponding to that of the binary orbit ( $\sim 50^\circ$ : Brandi et al. 2007; Quiroga et al. 2003) provides a significantly worse fit than a face-on ring or sphere. These results are based on simulated VLBA observations of circular and elliptical rings of various thicknesses and axis ratios, with brightness distributions around the ring similar to that observed. These simulations take account of such important interferometric uncertainties as the effects of limited uv-coverage and non-linear processing, including deconvolution in particular.

The ring center (as measured at 5 GHz on both days) at (J2000) is:

$$17^h50^m13^s.1583, -06^\circ42'28''.517,$$

with an uncertainty of at most one milliarcsecond (mas). We checked for systematic errors in our astrometry by phase referencing our secondary calibrator (J1743–0350) to our primary calibrator (J1745–0753) at 5 GHz. The resulting position agreed with that given in the ICRF to 0.4 mas in right ascension and 0.6 mas in declination – well within the  $1\sigma$  error bars reported in the ICRF. Since these calibrators are  $\sim 4^\circ$  apart, while RS Oph is separated from the primary calibrator by only  $1.67^\circ$ , systematic errors are far below other uncertainties in the measurement. Our VLBI position for RS Oph is however  $\sim 100$  mas from the optical position from the Naval Observatory Merged Astrometric Dataset (NOMAD; Zacharias et al. 2004):  $17^h50^m13^s.1628 \pm 9$  mas,  $-06^\circ42'28''.496 \pm 11$  mas. This optical position corrects for proper motion to the epoch 2006.19, and is shown as a cross in Fig. 1. There is no obvious explanation for the radio/optical offset.

The width of the ring is barely resolved in the first epoch, and clearly resolved in the second, suggesting a growing thickness with time. We fit the observed ring as a circle with an asymmetric brightness distribution, thickened by convolution with a symmetric Gaussian, and then convolved with the beam (point spread function). The full-widths-at-half-maxima (FWHMs) for the smoothing gaussians were  $2.5_{-2.5}^{+1.0}$  mas on the first day, and  $4.5 \pm 0.5$  mas on the second. The corresponding radii were  $16.25 \pm 0.5$  mas and  $17.5 \pm 0.5$  mas. These radii refer to the mid-points of the annuli; the outermost parts of the rings (mid-point + FWHM, from the fits) are at  $\sim 17.5$  and  $\sim 19.7$  mas. The error bars quoted here are more nearly  $3\sigma$  than  $1\sigma$  errors, insofar as this has meaning for non-Gaussian error distributions, and the difference in widths is thus likely to be real.

The asymmetry of the ring is much more pronounced at 5 GHz than at 1.7 GHz. This difference is not an instrumental effect: simulating 5 GHz observations of the 1.7 GHz model

shows that the 5 GHz observations would have shown the western emission clearly, had it been as (relatively) strong as at 1.7 GHz. Thus the spectrum of the eastern part of the ring is *intrinsically* relatively flat, while that of the western part falls sharply with frequency. Based on the simulations, we multiplied the observed flux density at 5 GHz by a factor 1.07 on day 20.8, and 1.10 on day 26.8, as a first-order correction for the differing uv-coverage between 5 and 1.7 GHz.<sup>2</sup> The resulting flux densities at 1.7 and 5 GHz are given in Table 1.

## 2.2. The Eastern Component

Our second set of observations revealed an additional component  $\sim 52$  mas to the east of the center of the ring. This new eastern component was present at both 1.7 and 5.0 GHz. The 1.7 GHz emission at this location is clearly resolved in the north/south direction, with a Gaussian fit yielding a rough deconvolved size of  $23.7 \pm 2.2$  mas ( $58.0 \pm 5.4$  AU at 2.45 kpc [see §3.1.2 for a derivation of the distance]). As with the ring, we simulated 5.0 GHz observations of the 1.7 GHz model, and found that, while the eastern component would appear much smaller at 5.0 GHz (as observed), the source spectrum must be intrinsically quite steep (see Table 1).

This component was not seen in our first set of observations. The 1.7 GHz map shows no source to the east of the ring: the  $5\sigma$  flux density upper limit is  $0.6$  mJy beam<sup>-1</sup>, compared to the peak flux density on March 11 of  $1.3$  mJy beam<sup>-1</sup>. The  $3\sigma$  5 GHz upper limit is approximately  $1$  mJy beam<sup>-1</sup>. Further VLBA observations on 2006 Mar 18 through 29 clearly detect the eastern component; we postpone discussion of those data to a future paper.

## 3. Discussion

### 3.1. The Ring

#### 3.1.1. Expansion Rate and Shape

The expanding ring is most naturally associated with the shock wave resulting from the outburst, and seen in the strong early X-ray emission (e.g., Sokoloski et al. 2006; Osborne et al. 2006a; Bode et al. 2006b) and broad optical, infrared, and X-ray lines (e.g., Buil 2006; Ness et al. 2006; Das et al. 2006b). Those data suggest substantial deceleration, as expected for a shock sweeping up more and more of the red giant’s stellar wind. Figure 3 compares

---

<sup>2</sup>Figures 1 and 2 do *not* reflect this correction, as it is very likely to vary with position.

the radius thus predicted from the optical, IR, and X-ray velocities with that observed in the radio. The solid circles represent outer radius estimates from the current data, derived through simulations of thick, asymmetric rings as discussed in §2.1. The open triangles represent the radii of O’Brien et al. (2006c), measured as half the maximum distance between peaks in a series of north-south slices. The nominal error bars of O’Brien et al. (2006c) are 0.2 mas, but, as they point out, these nominal errors almost certainly underestimate the true ones, and we plot 1 mas error bars in the figure. The systematic difference between O’Brien et al.’s measurements and ours, with the former lying some 20% low, is likely due to the differences in fitting procedures, combined with an evolving surface brightness distribution and changing angular resolution (cf. §5.6 of Bartel et al. 2002). Nonetheless, the overall trend of radio radius with time, as measured by either group, matches the X-ray/optical/infrared predictions nicely. The agreement between the size of the radio ring and the expected location of the blastwave also support the conclusion that, unlike the IR continuum emission, which primarily emanates from a region within a few mas of the central binary (Monnier et al. 2006; Lane et al. 2007), the radio emission is associated with the expanding shock.

As shown in Fig. 2, the ring is basically circular. This geometry is consistent with a spherical shock projected onto the plane of the sky (see, for instance, Bartel et al. 2002, for similar observations of supernova 1993J) or a two-dimensional shock in the plane of the sky. There is no evidence in the ring shape either for an asymmetric explosion or for any special geometry of the circumstellar material. In particular, we see no sign that the ring is inclined either parallel or perpendicular to the binary orbit ( $\sim 50^\circ$ : Brandi et al. 2007; Quiroga et al. 2003). The fractional width of the ring (thickness divided by radius) increases from  $0.15^{+0.06}_{-0.15}$  on day 20.8, to  $0.26 \pm 0.03$  on day 26.8 ( $\sim 3\sigma$  error bars). This breadth suggests that the emission arises in the forward rather than the reverse shock, since the latter is expected to be much thinner. The *change* in relative width shows that the evolution is *not* scale-free, thus ruling out a common theoretical simplification (e.g., Chevalier 1982).

### 3.1.2. Distance

Comparing the angular size observed by VLBI with the radius inferred from optical, X-ray, and infrared observations gives a direct estimate of the distance to the remnant. Three estimates of the evolving shock velocity are currently available.

First, the earliest optical spectra give initial velocities of  $3500 \pm 150 \text{ km s}^{-1}$  (based on Buil 2006, and early spectra reported on VSNet), which we take as constant between the explosion (assumed to occur on Feb.  $12.6 \pm 0.15$ , or  $\Delta t \equiv t - t_0 = -0.23 \pm 0.15$  days with respect to  $t_0$ , the time of optical maximum [Feb. 12.83]) and  $\Delta t = 1.47$  days.

Second, shock velocities may be derived from the observed X-ray temperatures, using the standard strong shock approximation and assuming the standard mean molecular weight ( $\mu = 0.6$ ) for a fully ionized plasma. The X-ray emission is clearly complex, with indications of multiple temperatures and densities present at any given time. Here we are interested in the highest temperature gas, corresponding to the material heated by the decelerating shock shown in the radio images, and adopt single-temperature fits to the highest energy X-rays seen in a given observation. The X-ray temperatures at early times, when the temperatures are highest, are best determined by the *Rossi X-ray Timing Explorer* (RXTE; Sokoloski et al. 2006), which responds most efficiently to higher-energy photons; at late times, as the shock slows and the corresponding temperature decreases, the relatively soft response of *Swift* provides the more relevant spectral coverage (Bode et al. 2006b). We therefore use the measurements of Sokoloski et al. (2006) before day 14.5, and those of Bode et al. (2006b) after day 13.5. The X-ray velocities are well fit by two independent power laws, as detailed in Table 2 and shown by the dashed lines in Fig. 4.

The third and final set of velocity estimates comes from infrared spectroscopy. Das et al. (2006b) measured the (deconvolved) full-widths at half maxima (FWHMs) and half-widths at zero intensity (HWZIs) of the observed line profiles of two infrared lines, O I and Pa $\beta$ , from 1.16 to 47.04 days after the explosion. While the measurements for the two lines are in rough agreement, and the FWHMs agree with the optical and X-ray velocities discussed above, the FWHMs for both lines – and the velocities inferred from the optical and X-ray data – are systematically low (by a factor  $\sim 1.7$ ) compared with the FWZI. This discrepancy was also noted by Evans et al. (2007). Fig. 2 of that paper shows that the difference between FWHM and HWZI results from the shape of the line profile: a strong, narrow, roughly Gaussian peak, surrounded by a faint, broad plateau. The narrow component suggests an expanding wind or outflow, while the broad plateau is more characteristic of a thin shell (e.g., Lynch et al. 2006; Bertout & Magnan 1987; Gill & O’Brien 1999). The consistent ratio of the FWHMs and HWZIs, and the roughly constant ratio of the peak flux density in the two components, shows they remain closely associated for at least the first 40 days after the explosion.

The early optical reports may well have missed a faint, broad line component. The much lower velocities derived from the X-ray temperatures, and their agreement with the FWHM of the narrow component of the infrared lines, is more puzzling. Tatischeff & Hernanz (2007) suggest that cosmic ray acceleration at the blast wave may explain both the velocity discrepancy and the relatively rapid deceleration of the shock.

Here we assume the broad component of the infrared lines represents the shock velocity, as both the line shape and the extreme velocity suggest a thin, rapidly expanding shell. The scatter in the infrared measurements from day to day suggests some short-lived physical

effects, or some uncertainty in the determinations of the line widths.<sup>3</sup> We therefore multiply the smooth fit to the X-ray and optical velocities (see above) by 1.7, to give a smooth curve which roughly reproduces the decline in the infrared HWZI. With these assumptions, the errors on the shock radii at the times of our VLBA observations are dominated by the error on the time of the explosion.

Comparing these radii to the angular sizes corresponding to the outer part of the shock ( $\theta = 17.5 \pm 0.5$  mas at  $\Delta t = 20.8$  days;  $\theta = 19.7 \pm 0.5$  mas for  $\Delta t = 26.8$  days) gives two fairly independent measurements of the distance:

$$D_{20.8} = r_{20.8}/\theta_{20.8} = 2.392 \pm 0.078 \text{ kpc}$$

$$D_{26.8} = r_{26.8}/\theta_{26.8} = 2.492 \pm 0.071 \text{ kpc}$$

where the error bars are statistical, and dominated by the uncertainties in  $\theta$ . Taking the weighted average of these two distances gives a distance of  $2.45 \pm 0.05$  kpc.

The major uncertainty in this estimate lies in the relation between the sizes measured with VLBI, and the velocities inferred from other wavelengths. First, if the ring is a two-dimensional structure inclined at an angle  $i$  to the line-of-sight, that will increase the quoted distances by  $1/\cos i$ : a factor 1.6 for  $i = 50^\circ$ . Given the observed circularity of the ring, this is likely to be a  $< 10\%$  effect. Second, we have assumed that the infrared velocities reflect those of the leading edge of the radio emission. Adding an additional 10% (rms) systematic uncertainty based on the possibility that the outer edge of the observed radio shock lies within the high-velocity region traced by the extreme infrared velocities, the final distance estimate is then  $2.45 \pm 0.05 \pm 0.37$  kpc, where the first error bars refers to the random and the second to the systematic errors.

Previous distance estimates are summarized by Bode (1987); see also Barry et al. (in prep.). These were based on spectral luminosity determinations, the presence or absence of absorption features at known distances, and a very rough relation between the distance and (cold) H I column density (see primarily Hjellming et al. 1986). Bode (1987) concluded that the distance was likely to be around  $1.6 \pm 0.3$  kpc. Our more direct estimate is higher but not enormously so. Further, since a significant inclination for the ring can only *increase* our distance estimate, the comparison implies again that the ring is nearly face-on.

---

<sup>3</sup>Fig. 2 of Das et al. (2006b) shows error bars which appear sufficient to explain much of the scatter, but those error estimates are not given explicitly in the text or in Table 2 of that paper.

### 3.1.3. Emission and Absorption

Given the close agreement between the blast wave velocity evolution inferred from X-ray, optical, and infrared observations and the expansion of the radio ring, it seems worth checking whether a significant fraction of the radio flux density could be thermal bremsstrahlung from the X-ray-emitting gas. Fits to the data of Bode et al. (2006b) (Table 2) give the temperature of the post-shock gas as  $\sim 2.4 \times 10^7$  K on day 20.8 and  $\sim 1.8 \times 10^7$  K on day 26.8. These plasma temperatures are close to the observed peak surface brightness, which corresponds to an optically-thick black body of a few times  $10^7$  K. However, a mass of more than  $10^{-5} M_{\odot}$  would be required to make the thermal gas optically thick in the radio, and the corresponding thermal energy would be more than  $10^{44}$  ergs – an order of magnitude above the total energy of the outburst (e.g., Hachisu & Kato 2001; Sokoloski et al. 2006) – with a correspondingly high X-ray luminosity. Clumping of higher-temperature gas would reduce the required mass somewhat, but not enough to remove these difficulties. Thermal emission is thus unlikely to play a major role in the few-GHz radio flux at this stage of the outburst.

The obvious alternative is synchrotron emission, which can easily explain the observed high surface brightness. Optically-thin synchrotron spectra generally range from  $\nu^{-0.6}$  to  $\nu^{-1}$ , providing a natural explanation for the  $\sim \nu^{-0.7}$  spectrum of the western side of the ring. The eastern part of the ring, with  $\alpha = -0.20 \pm 0.02$  ( $S_{\nu} \propto \nu^{\alpha}$ ) on day 20.8 and  $\alpha = -0.27 \pm 0.01$  on day 26.8, is more puzzling. Foreground absorption in a  $1/r^2$  medium would be expected to change rapidly over this time period, while the observed spectrum is fairly constant. Also, whereas any foreground absorption (or synchrotron self-absorption) should have caused the flux density to decrease with decreasing frequency below 1.7 GHz, in fact the 0.61 GHz flux density of  $48 \pm 2$  mJy on day 20.3 (Anupama & Kantharia 2006) was higher than the 1.7 GHz flux density of  $36.7 \pm 0.3$  mJy that we measured from the eastern part of the ring on day 20.8. Either the eastern side of the ring contains a complicated mix of emission and absorption, or the spectrum reflects a very unusual energy distribution of relativistic particles.

Assuming the emission is synchrotron – a conclusion shared by O’Brien et al. (2006c) – standard equipartition arguments (e.g., Burbidge 1959) suggest minimum energies in relativistic particles and fields of  $\sim 10^{41} (1+k)^{4/7}$  ergs, where  $k$  is the ratio of the energy in protons to that in electrons;  $k \sim 100$  is observed locally, while  $k \sim 40$  is predicted for strong shocks (e.g., Beck & Krause 2005). The equipartition magnetic field at the location of the peak flux density in the ring is of order  $0.03 (1+k)^{2/7}$  G, comparable to previous results based on much lower quality data (Bode & Kahn 1985; Taylor et al. 1989). The corresponding magnetic pressure is  $2.7 \times 10^{-5}$  dyn cm $^{-2}$ . As expected, these values are well below the total energy and pressure in the shock front.

### 3.2. The Eastern Component

#### 3.2.1. Emission Mechanism and Speed

The steep spectral index ( $\alpha \sim -0.67$ ) and high surface brightness ( $T_B \sim 10^7$  K at 1.7 GHz) of the eastern component indicate that the emission must be primarily synchrotron. The minimum (equipartition) energy is then  $\sim 0.15 \times 10^{41} (1+k)^{4/7}$  ergs, a factor 10 below that in the ring, while the corresponding equipartition magnetic field is comparable,  $\sim 0.03 (1+k)^{2/7}$  G.

If this component was ejected from the source at the core of the expanding ring, it is moving quite rapidly. Presumably it was ejected during or after the initial outburst, and is thus at most 27 days old when first detected by us (2006 Mar 11). At a distance of  $\sim 52$  mas from the center of the ring, its projected velocity is  $\gtrsim 2$  mas day $^{-1}$ , which corresponds to  $\gtrsim 8500/\sin i$  km s $^{-1}$  (where  $i$  is the inclination to the line-of-sight, and taking a distance of 2.45 kpc). For an inclination  $i \sim 50^\circ$ , the velocity of the eastern component is  $\sim 11,000$  km s $^{-1}$ . For comparison, the escape speed from a white dwarf is  $\sim 6530(1 - M/1.456 M_\odot)^{-1/4}$  km s $^{-1}$  (Hansen & Kawaler 1994), or  $\sim 12,600$  km s $^{-1}$  for  $M = 1.35 M_\odot$ . Based on the contour plot of O’Brien et al. (2006c), the EVN detection on day 21.5 gives roughly the same speed. The eastern component had thus not decelerated significantly before day 27.

#### 3.2.2. First Appearance

O’Brien et al. (2006c) present a preliminary view of VLBA, EVN, and MERLIN observations of RS Oph in 2006, with the VLBI data covering days 13.8–28.7. Most aspects of our images agree reasonably well with their results. However, they detect the eastern component quite strongly (peak  $\sim 0.8$  mJy beam $^{-1}$ ) at 5 GHz with the EVN on day 21.5, while we do *not* see that component with the VLBA on day 20.8. This apparent discrepancy is likely due to the more centrally concentrated uv-coverage of the EVN observations, which are correspondingly more sensitive to faint, extended emission. The eastern component was therefore already extended by day 20.8, as we directly observe on day 26.8. Further, our detection of the component at 5 GHz with the same instrument and observing time on day 26.8 as our non-detection on day 20.8 shows that the eastern component was still brightening during this time.

Our 1.7 GHz VLBA observations on day 20.8 do not show the eastern component. This result agrees with the non-detection of O’Brien et al. (2006) at the same frequency on day

20.5. Since the VLBA is much more sensitive to extended structures at this lower frequency than at 5 GHz (the angular response scales as  $\lambda/B$ , with  $\lambda$  the wavelength, and  $B$  the length of the baseline under consideration), our non-detection at 1.7 GHz places strong constraints on the spectrum around day 21. Had the spectrum on day 21 been as steep as the spectrum we observed on day 27, we would have measured a 1.7 GHz flux density of  $\gtrsim 1.7$  mJy, or  $\gtrsim 10\sigma$  in our VLBA observations. Considering instead the  $5\sigma$  upper limit of 0.6 mJy/beam at 1.7 GHz, and comparing this limit to the EVN detection, we find that on day 21, the radio spectrum was actually either flat or inverted (rising towards higher frequencies). The eastern-component spectrum therefore evolved significantly between day 21 and day 27.

### 3.2.3. Absorption

The spectral and flux density evolution, combined with the inferred large extent of the eastern component, suggest that external (free-free) absorption is important, as expected for a source embedded in a dense, ionized red giant wind. The primary challenge lies in explaining the initial obscuration of the eastern component at a time when the ring is clearly visible. O’Brien et al. (2006c) invoke a special geometry to explain the visibility of the ring, as well as the late turn-on of the eastern component and the lack of any corresponding western feature during the first month. In their picture, the obscuring medium is the circumstellar material (assumed spherically symmetric) shed by the red giant companion. They assume the radio emission comes from a bright, slowly expanding equatorial ring and a bipolar shock structure. They take the approaching (eastern) side of the bipolar jet to be inclined about  $30^\circ$  to the line-of-sight, moving outward, and sweeping up absorbing material. In this picture, the eastern component of the jet becomes visible when the shock overtakes most of the absorbing circumstellar material. The receding jet remains behind more of the red giant wind, so that (western) component is not expected to be seen until later. They suggest that the more distant (eastern) part of the ring is visible almost instantly because the jet has swept away the densest, high-obscuration part of the red giant wind along that line-of-sight.

One can make this more quantitative by requiring that the free-free opacity  $\tau$  due to the red giant wind be  $\gtrsim 1$  at the times and frequencies where the eastern component is not seen, and  $\lesssim 1$  at the times and frequencies where it is. The opacity predicted for a fully ionized, spherically symmetric,  $1/r^2$  wind are shown as a function of projected distance from the center in Fig. 5, together with arrows showing the rough constraints from the 1.7 and 5 GHz VLBI observations. This simple model works remarkably well. Assuming one proton per electron and an electron temperature of  $10^4$  K, and taking the wind velocity  $v_w = 20$  km s $^{-1}$ , the inferred mass loss rate is  $\sim 1 \times 10^{-6} M_\odot$  yr $^{-1}$  for an inclination  $i \sim 50^\circ$  for the eastern

component’s velocity vector. This mass loss rate is quite reasonable, and within a factor of two of that derived by O’Brien, Bode, & Kahn (1992) (after correcting for the difference in the assumed distance) based on shock models fit to the X-ray emission from the 1985 outburst.

Absorption can thus easily explain the late appearance of the eastern component; but the central ring is more challenging. In the O’Brien et al. (2006c) model, the observed ring should represent the projection of a highly-inclined, two-dimensional circle, i.e., an ellipse. Our data show that the ring in fact is quite circular (Fig. 2), making explanations involving strong deviations from spherical symmetry difficult to maintain. The flat spectrum of the eastern part of the ring is also not a natural result of the O’Brien et al. (2006c) model.

Another possible explanation for the abrupt appearance of the eastern component is that it was intrinsically faint until around day 21. The eastern component could represent a terminal shock of the kind associated with the ejecta of many active galactic nuclei, micro-quasars, and protostars (in the form of Herbig Haro objects), although this explanation has some difficulties since for RS Oph, the circum-binary density falls off rapidly with distance rather than abruptly increasing.

The ejecta could also have brightened upon moving into the relative vacuum beyond the outer edge of the wind nebula. As in the current outburst, the expanding shock in 1985 swept up the CSM, leaving behind a relative vacuum. Over the past 21 years, the red giant has been re-filling this vacuum with a wind moving out at  $\sim 20 \text{ km s}^{-1}$  (Wallerstein 1958; Dufay et al. 1964; Gorbatskiii 1972). The collimated ejecta would have reached the edge of this re-filled region in  $\sim 14 \text{ days } (v_w/20 \text{ km s}^{-1}) (v_{jet}/11,000 \text{ km s}^{-1})^{-1}$  (where  $v_{jet}$  is the velocity of the collimated outflow), around the same time that it brightened in the radio. If the red giant wind can carry outward and compress (and hence strengthen) the magnetic field at large radii, relativistic particles might produce copious synchrotron emission upon encountering the compressed field. Alternatively, if the relativistic plasma was initially highly confined by the circumstellar gas (and thus synchrotron self-absorbed), it might expand and become visible at lower radio frequencies upon reaching the edge of the confining medium.<sup>4</sup> One might then expect the eastern component to become relatively stationary at late times rather than continuing to move out rapidly.

---

<sup>4</sup>Note that the azimuthal extent of the eastern component requires a fairly wide-angle ‘jet’. If the jet were intrinsically narrow until reaching the edge of the red giant wind, the azimuthal velocity would have to be  $\gtrsim 17,000 \text{ km s}^{-1}$  to match the observed azimuthal extent on day 21.

#### 4. Conclusions

Dual-frequency VLBA observations made 20.8 and 26.8 days after the February 2006 outburst of the recurrent nova RS Oph have shown that the bulk of the radio emission at this stage comes from an expanding synchrotron shell. The shell’s increasing angular size matches the shock velocities inferred from X-ray observations and measured through infrared spectroscopy, confirming the basic picture of a decelerating shock between the material flung off in the explosion from the surface of the white dwarf and the circumstellar material produced by the wind of its red giant companion. This gives a direct distance estimate of  $\sim 2.45 \pm 0.05 \pm 0.37$  kpc, the most accurate yet determined for this source.

This evolving shock is far from simple. The shell evolution is *not* self-similar, with the shell thickness increasing from  $\sim 15\%$  to  $\sim 26\%$  between the two epochs. In addition, the brightness distribution around the shell is highly asymmetric, with the eastern side many times brighter than the western side. The eastern side of the ring also has a much flatter radio spectrum. To our knowledge, such a spectrum has been seen only once before for a high-brightness resolved source, in the radio images of the expanding shell associated with the peculiar X-ray outburst of the emission-line star CI Cam (Mioduszewski & Rupen 2004). Finally, the flux density of the western part of the shell is *increasing* with time, in contrast to the optically-thin behavior of the ejecta-driven shocks in physically similar systems such as supernovae (e.g., Weiler et al. 2002).

Our VLBA images also reveal an additional eastern component that is well separated from the dominant ring. ‘Jets’ (generally just elongations or separate components in barely-resolved sources) have been seen in previous outbursts of this and other symbiotic stars. The VLBI observations of RS Oph constitute the first unambiguous evidence for a synchrotron jet emanating from a white dwarf system. The inferred speed is close to the escape speed from a high-mass white dwarf, in accord with the generally good agreement between directed outflow and escape speeds for physical systems ranging from low-mass protostars to black hole binaries and active galactic nuclei<sup>5</sup>. Similarly, synchrotron emission is characteristic of fast jets, where emission far from the powering source is generally assumed to derive from an interaction between the flow and the surrounding medium. The association of a highly directed and a quasi-spherical outflow is more unusual, but certainly not unprecedented; for instance, the jet model for gamma-ray bursts, and their association with core-collapse supernovae (e.g., MacFadyen & Woosley 1999), has brought the physical connection between quasi-spherical and highly directed outbursts into much greater prominence.

---

<sup>5</sup>In supernovae and gamma-ray bursts, the relevant escape speeds are those of the compact objects which are formed, not those of the progenitor stars.

The eastern component that was so prominent on day 27 appeared to “turn on” around day 21. Although this turn-on could be due to decreasing absorption by the circumstellar medium as the eastern component moved outwards, there are several difficulties with this picture. Intrinsic brightening, possibly associated with the component reaching the edge of the region re-filled by the red giant wind since the last nova outburst in 1985, may also play a role in the turn-on.

The preferred east-west axis for the observed asymmetries is consistent with VLBI observations on day 77 of the last (1985) outburst, which showed a strong east/west extension (Taylor et al. 1989). The persistent east-west asymmetry suggests that this preferred axis reflects an intrinsic asymmetry in the binary system, rather than (for instance) some statistical irregularity in a particular explosive event. The binary orbit provides one possible source of the asymmetry. Although a highly anisotropic density structure around the binary could collimate the outflow, with the ‘jet’ naturally focused along the axis of least resistance (cf. Lloyd et al. 1993), one would then expect the observed ring to correspond to the high-density ‘waist’ of this structure. The ring is in fact circular in projection and brightest along the trajectory of the eastern component. Whatever the collimation mechanism in RS Oph, we may for the first time be seeing the formation of a white-dwarf jet, as well as the most compelling demonstration to date of both its high initial speed and the physical emission mechanism (synchrotron emission).

We are grateful to the VLBA scheduling committee and the array operations staff for the efforts which made these observations possible. As with most research on bright variable stars, this work has greatly benefited from the regular monitoring (and quick reporting) of both amateur and professional variable star observers, generally publicized through the American Association of Variable Star Observers (AAVSO) and the Variable Star Network (VSNet). We are further grateful to the referee, Mike Bode, for a number of useful comments, as well as for organizing an exceptionally productive workshop on this source in the summer of 2007. J.L.S. is supported by an NSF Astronomy and Astrophysics Postdoctoral Fellowship under award AST 03-02055. This research has made use of NASA’s Astrophysics Data System; the SIMBAD database, operated at CDS, Strasbourg, France; and the USNOFS Image and Catalogue Archive, operated by the United States Naval Observatory, Flagstaff Station (<http://www.nofs.navy.mil/data/fchpix/>).

*Facilities:* VLBA ().

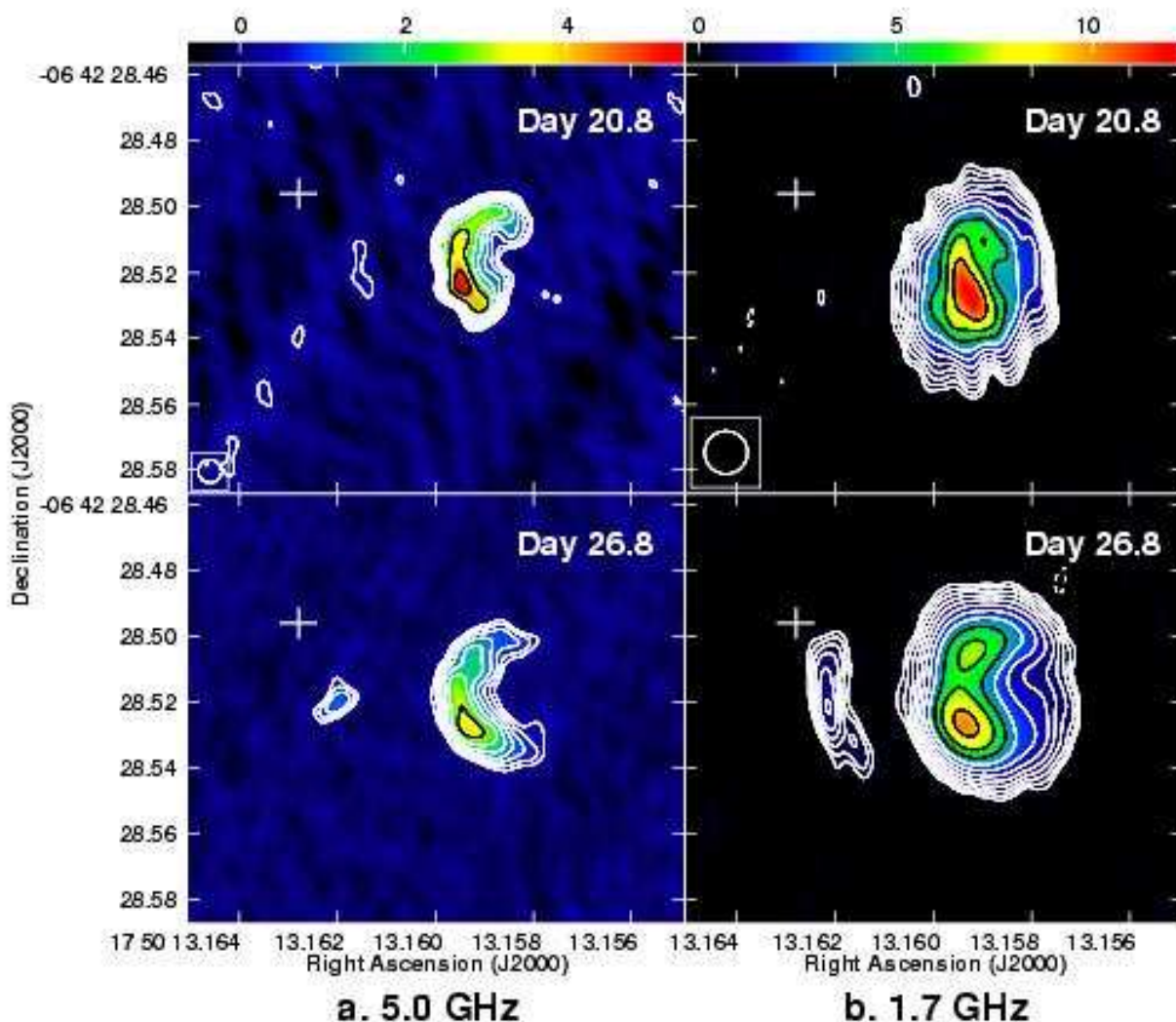


Fig. 1.— VLBA total intensity images of RS Oph, from 2006 March 5 (day 20.8; upper) and 2006 March 11 (day 26.8; lower). (a) 5.0 GHz images (left column), convolved to a resolution of  $7.6 \times 7.6$  mas. Contours are  $\pm 0.25 \text{ mJy beam}^{-1} \times 2^{n/2}$ ,  $n = 2, 3, \dots$ , and the color scale ranges from 0 to 6  $\text{mJy beam}^{-1}$ . The peak flux densities in the two images are  $5.9 \pm 0.25 \text{ mJy beam}^{-1}$  on day 20.8, and  $4.3 \pm 0.11 \text{ mJy beam}^{-1}$  on day 26.8. Note that the 5.0 GHz images are inherently less sensitive to large structures, due to the difference in interferometric baseline coverage as measured in wavelengths. The total 5.0 GHz flux densities, uncorrected for this effect, are 41.3 and 26.3 mJy. (b) 1.7 GHz images (right column), convolved to a resolution of  $13 \times 13$  mas. Contours are  $\pm 0.12 \text{ mJy beam}^{-1} \times 2^{n/2}$ ,  $n = 2, 3, \dots$ , and the color scale ranges from 0 to 13  $\text{mJy beam}^{-1}$ . The peak flux densities in the two images are  $13.0 \pm 0.12 \text{ mJy beam}^{-1}$  on day 20.8, and  $10.3 \pm 0.13 \text{ mJy beam}^{-1}$  on day 26.8, with the error bar reflecting the off-source rms noise. The total flux densities are 43.1 and 30.1 mJy. The cross to the northeast in each panel marks the optical position of RS Oph, from NOMAD (see § 2.1); the size of the cross represents the NOMAD error bars.

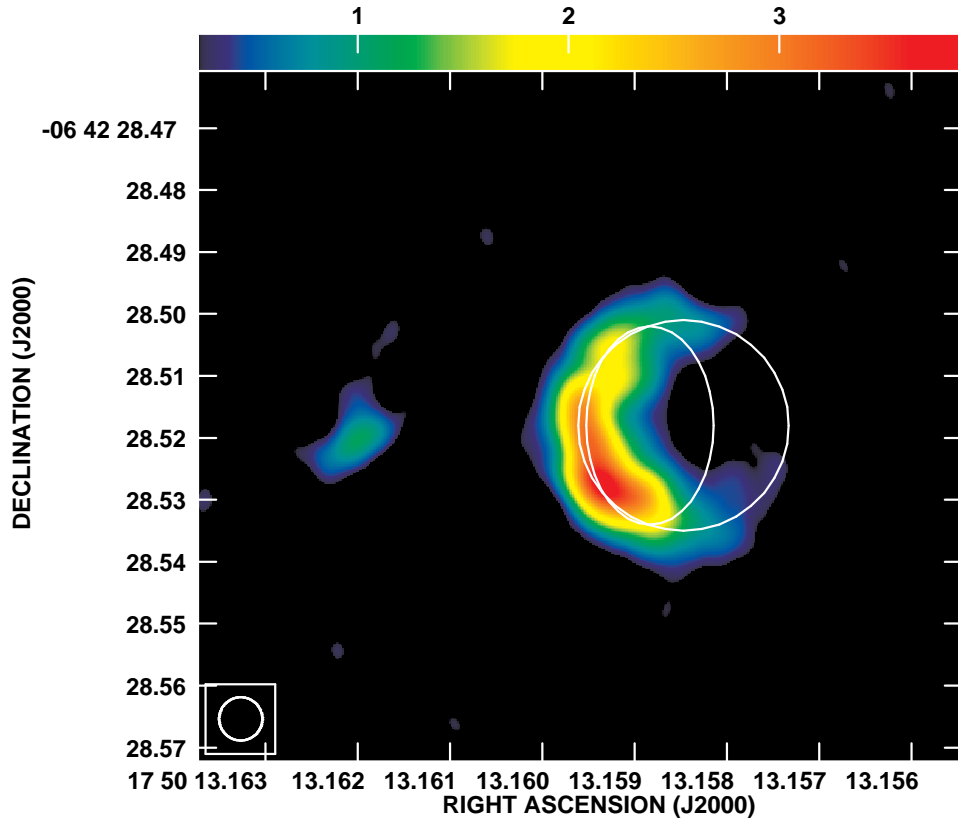


Fig. 2.— Tilted circular rings superposed on the 5.0 GHz image from day 20.8, for inclinations of  $0^\circ$  (face-on) and  $50^\circ$ , using radii of 31 and 29 milliarcseconds, respectively. The orbital inclination is thought to be  $\sim 50^\circ$  (Quiroga et al. 2003; Brandi et al. 2007). The color scale for the image ranges from 0.25 (black) to 3.865 (red)  $\text{mJy beam}^{-1}$ .

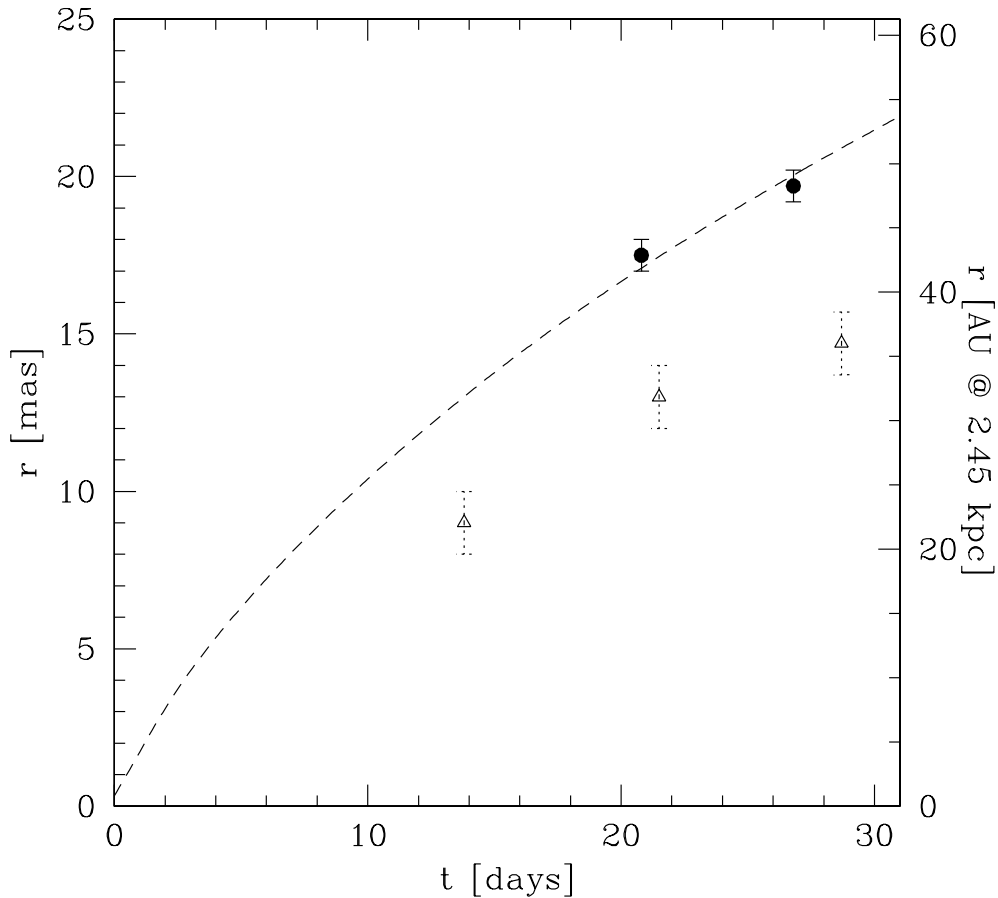


Fig. 3.— The radius of the ring as a function of time since the optical peak on 12.83 Feb 2006 UT. The solid circles represent the outer radii of the fit annuli (see text). The triangles shows the data of O’Brien et al. (2006c), assuming a 1 mas error bar (see text); these size estimates are only approximate, and the disagreement between the two groups is likely due to differences in the methods of their derivations (e.g., it is likely that O’Brien et al. (2006c)’s values refer to the mid-point rather than the outer edge of the ring). The dashed line shows the expansion detailed in Table 2, scaled up by a factor 1.7 to match the width of the broad infrared spectral component (see § 3.1.2).

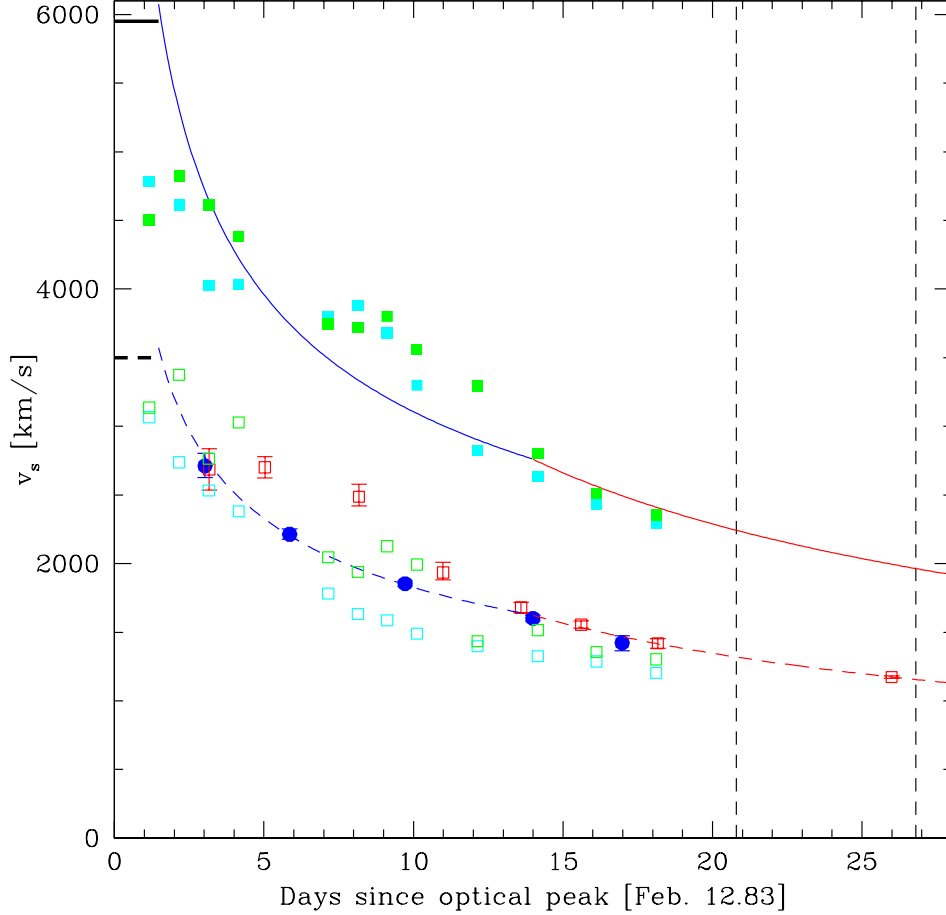


Fig. 4.— The velocity of the shock vs. time, as derived from infrared, optical, and X-ray data. The observed widths of the O I line are shown in green, and those of the Pa $\beta$  line in light blue (cyan); the open squares represent the full-widths at half-maximum, and the solid squares show the half-widths at zero intensity (HWZIs). The blue dots and error bars are shock velocities inferred from *RXTE* X-ray data in Sokoloski et al. (2006), while the red ones are similarly derived from *Swift* X-ray data in Bode et al. (2006b). The blue and red dashed curves represent power-law fits (see Table 2) to the observed X-ray velocities, ignoring data from Sokoloski et al. (2006) taken after day 14.5, and data from Bode et al. (2006b) taken before day 13.5. The dashed black horizontal line shows the velocity for the earliest part of the outburst, taken from early optical reports. As discussed in § 3.1.2, the solid black, blue, and red curves show the result of multiplying the X-ray and optical fits by 1.7, to match the infrared HWZIs. These solid curves represent our best estimate of the shock velocity. The vertical dashed lines show the dates of our VLBA observations.

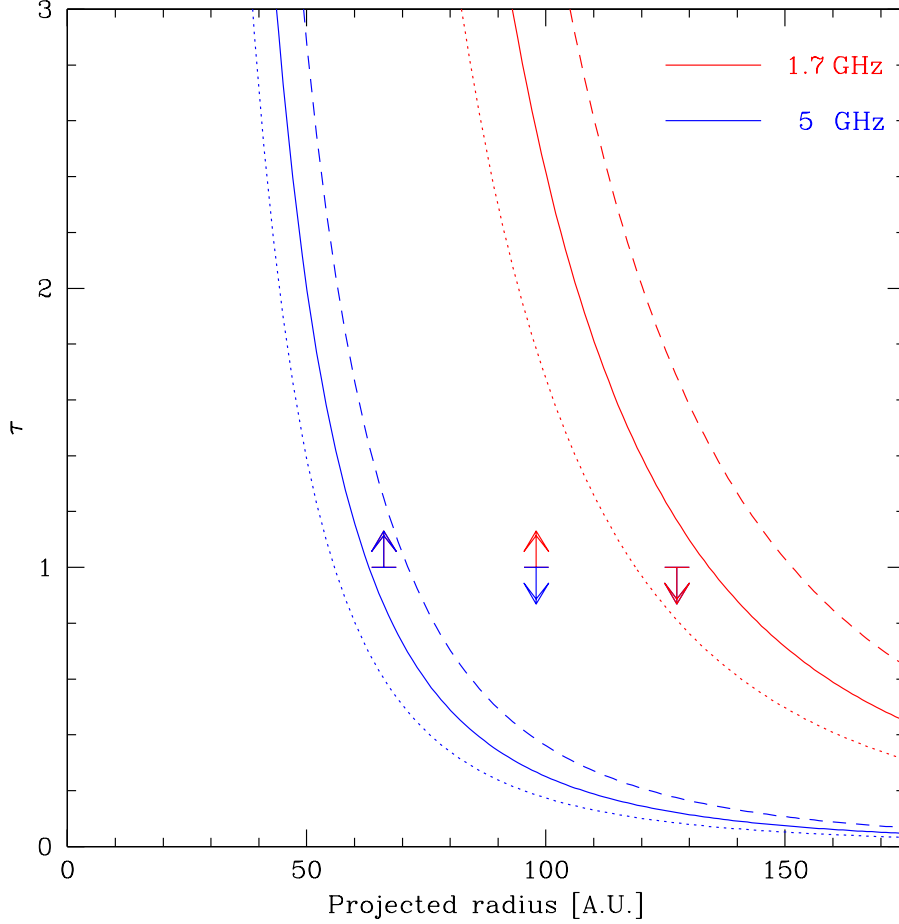


Fig. 5.— The free-free opacity predicted for a  $1/r^2$  wind from the red giant, at 5 GHz (blue) and 1.7 GHz (red), as a function of the (observed) projected distance from the red giant. The red and blue arrows show the rough constraints from the VLBI imaging of the eastern component — the opacity must be  $\lesssim 1$  when that component is not detected, and  $\gtrsim 1$  when it is detected. The horizontal placement of these limits assumes  $D = 2.45$  kpc; a smaller distance would shift these to the left (implying a lower  $\dot{M}/v_w$ ), while a larger distance would shift these to the right (implying a higher  $\dot{M}/v_w$ ). The solid curves show a rough fit to these limits, corresponding to  $\dot{M}/v_w = 1 \times 10^{-6} M_\odot \text{ yr}^{-1} / 20 \text{ km s}^{-1}$  for an inclination of  $i \sim 50^\circ$ . The dotted lines show the opacities for a 20% lower  $\dot{M}/v_w$ , while the dashed lines show the opacities for a 20% higher value. These calculations take the electron temperature to be  $10^4$  K, and assume one proton per electron.

Table 1.

| Epoch       | Feature             | $S_{1.7}^a$<br>(mJy beam $^{-1}$ ) | $S_{corr,5.0}^b$<br>(mJy beam $^{-1}$ ) | $\alpha^c$       |
|-------------|---------------------|------------------------------------|---|------------------|
| 2006 Mar 05 | Entire ring         | $43.1 \pm 0.3$                     | $32.2 \pm 0.6$                          | $-0.27 \pm 0.02$ |
|             | Ring-E <sup>d</sup> | $36.7 \pm 0.3$                     | $29.5 \pm 0.6$                          | $-0.20 \pm 0.02$ |
|             | Ring-W <sup>d</sup> | $6.4 \pm 0.3$                      | $2.8 \pm 0.6$                           | $-0.76 \pm 0.20$ |
| 2006 Mar 11 | Entire ring         | $41.3 \pm 0.2$                     | $28.8 \pm 0.2$                          | $-0.33 \pm 0.01$ |
|             | Ring-E <sup>d</sup> | $33.3 \pm 0.2$                     | $24.8 \pm 0.2$                          | $-0.27 \pm 0.01$ |
|             | Ring-W <sup>d</sup> | $8.0 \pm 0.2$                      | $3.8 \pm 0.2$                           | $-0.67 \pm 0.01$ |
|             | E.C. <sup>d</sup>   | $4.2 \pm 0.2$                      | $1.9 \pm 0.2$                           | $-0.71 \pm 0.10$ |

<sup>a</sup>Flux density at 1.7 GHz.

<sup>b</sup>Flux density at 5.0 GHz, corrected for flux density missing as found by simulating 5.0 GHz observations of the 1.7 GHz model (see text). The observed flux densities have been multiplied by 1.07 on 2006 March 05, 1.10 for the ring on 2006 March 11, and 1.21 for the eastern component on 2006 March 11.

<sup>c</sup>Spectral index  $\alpha$ , with the flux density going as the frequency to this power ( $S_\nu \propto \nu^\alpha$ ).

<sup>d</sup>Ring-E refers to the eastern (bright) part, and Ring-W to the western (dim) part, of the ring. E.C. refers to the eastern component.

Table 2.

| Time covered by fit <sup>a</sup> |        | Fit parameters <sup>b</sup> |                            |                       |
|----------------------------------|--------|-----------------------------|----------------------------|-----------------------|
| $t_1$                            | $t_2$  | $R_{21}^c$                  | $\alpha^d$                 | $\chi^2/N_{d.o.f.}^e$ |
| (days)                           | (days) | (A.U.)                      |                            |                       |
| $-0.23 \pm 0.15$                 | 1.47   | $3.44 \pm 0.34$             | $\equiv 0.0$               | ...                   |
| 1.47                             | 14.0   | $15.49 \pm 0.17$            | $-0.350 \pm 0.018$         | 2.94/3                |
| 14.0                             | 20.8   | $5.70^{+0.039}_{-0.038}$    | $-0.524^{+0.022}_{-0.019}$ | 2.58/3                |
| 14.0                             | 26.8   | $9.96^{+0.063}_{-0.056}$    | $-0.524^{+0.022}_{-0.019}$ | 2.58/3                |
| $t_{expl}^f$                     | 20.8   | $24.63 \pm 0.38$            | ...                        | ...                   |
| $t_{expl}^f$                     | 26.8   | $28.89^{+0.38}_{-0.39}$     | ...                        | ...                   |

<sup>a</sup>Times  $t_1$  to  $t_2$  over which the fit holds, measured in days with respect to the time of optical maximum  $t_0 \equiv \text{Feb. 12.83}$ .

<sup>b</sup>Results of least-squares power-law fits to the X-ray data, parameterized in terms of the distance traversed by the shock  $R_{21}$ , and the power-law index  $\alpha$ . *Note that the distances have not yet been scaled to match the broad infrared spectral component* – see §3.1.2.

<sup>c</sup>The distance the shock has traveled between  $t_1$  and  $t_2$ , in astronomical units (A.U.). *Note that these distances have not yet been scaled to match the broad infrared spectral component* – see §3.1.2. Error bars are  $1\sigma$  based on standard propagation of errors, and are primarily statistical. The exception is the uncertainty in the explosion date ( $t_{expl} = -0.23 \pm 0.15$ ), which is a best guess as to the likely range of dates.

<sup>d</sup>The power-law index  $\alpha$  of a fit to the velocities:  $v \propto t^\alpha$ . Error bars are  $1\sigma$ .

<sup>e</sup> $\chi^2$  and the number of degrees-of-freedom for the fit. Note that  $\chi^2$  has *not* been normalized —  $\chi^2 \sim N_{d.o.f.}$  indicates a good fit.

<sup>f</sup>These rows give the total distance traveled between the (uncertain) date of the explosion  $t_{expl}$ , and the dates of our VLBA observations (20.8 and

26.8 days). The error bars are  $1\sigma$  based on a simple propagation of the error bars for each segment of the fit, assuming the error bars on the individual segments are independent. *Note that these distances have not yet been scaled to match the broad infrared spectral component – see § 3.1.2.*

Note. — The results given here have not yet been scaled to match the velocities measured for the broad infrared spectral component – see § 3.1.2.

## REFERENCES

- Anupama, G. C. & Kantharia, N. G. 2006, IAU Circ., 8687
- Bartel, N. et al. 2002, ApJ, 581, 404
- Bertout, C. & Magnan, C. 1987, A&A, 183, 319
- Bode, M. F. & Kahn, F. D. 1985, MNRAS, 217, 205
- Beck, R. & Krause, M. 2005, Astron. Nachr., 326, 414
- Bode, M. F. 1987, ed., RS Ophiuchi (1985) and the Recurrent Nova Phenomenon, Utrecht: VNU Science Press
- Bode, M. F., et al. 2006, IAU Circ., 8675
- Bode, M. F., et al. 2006, ApJ, 652, 629
- Brandi, E., Quiroga, C., Ferrer, O. E., Mikolajewska, J., & García, L. G. 2007, poster at the Keele University workshop on RS Ophiuchi 2006 (12-14 June 2007).
- Brocksopp, C., Bode, M. F., & Eyres, S. P. S. 2003, MNRAS, 344, 1264
- Brocksopp, C., Sokoloski, J. L., Kaiser, C., Richards, A. M., Muxlow, T. W. B., & Seymour, N. 2004, MNRAS, 347, 430
- Buil, C. 2006, CBET, 403
- Burbidge, G.R. 1959, ApJ, 129, 849
- Chevalier, R.A. 1982, ApJ, 258, 790
- Crocker, M. M., Davis, R. J., Eyres, S. P. S., Bode, M. F., Taylor, A. R., Skopal, A., & Kenny, H. T. 2001, MNRAS, 326, 781
- Das, R. K., Ashok, N. M., & Banerjee, D. P. K. 2006a, IAU Circ., 8673
- Das, R., Banerjee, D. P. K., & Ashok, N. M. 2006b, ApJ, 653, L141
- Davis, R. J. 1987, in RS Ophiuchi (1985) and the Recurrent Nova Phenomenon (ed. M.F. Bode), Utrecht: VNU Science Press, 187
- Dobrzycka, D. & Kenyon, S.J. 1994, AJ, 108, 2259
- Dufay, J., Bloch, M., Bertaud, C., & Dufay, M. 1964, Annales d’Astrophysique, 27, 555

- Evans, A. et al. 2006, IAU Circ., 8682
- Evans, A. et al. 2007, MNRAS, 374, L1
- Eyres, S. P. S., O’Brien, T. J., Muxlow, T. W. B., Bode, M. F., & Evans, A. 2006, IAU Circ., 8678
- Fey, A.L. et al. 2004, AJ, 127, 3587
- Fomalont, E., Petrov, L., McMillan, D.S., Gordon, D., & Ma, C. 2003, AJ, 129, 1163
- Galloway, D. K. & Sokoloski, J. L. 2004, ApJ, 613, L61
- Gill, C. D. & O’Brien, T. J. 1999, MNRAS, 307, 677
- Gonzalez-Riestra, R., Orio, M., & Leibowitz, E. 2006, IAU Circ., 8695
- Gorbatskii, V.G. 1972, Soviet Astronomy, 16, 32
- Greisen, E.W. 2003, in Information Handling in Astronomy – Historical Vistas, ed. A. Heck (Dordrecht: Kluwer Academic Publishers), 109
- Hachisu, I. & Kato, M. 2001, ApJ, 558, 323
- Hansen, C. J. & Kawaler, S. D. 1994, Stellar Interiors, New York: Springer-Verlag
- Hjellming, R. M., van Gorkom, J. H., Seaquist, E. R., Taylor, A. R., Padin, S., Davis, R. J., & Bode, M. F. 1986, ApJ, 305, L71
- Hog, E. et al. 2000, A&A, 355, L27
- Hollis, J. M., Pedelty, J. A., & Kafatos, M. 1997, ApJ, 490, 302
- Iijima, T. 2006, IAU Circ., 8675
- Iijima, T. & Essenoglu, H. H. 2003, A&A, 404, 997
- Kafatos, M., Hollis, J. M., Yusef-Zadeh, F., Michalitsianos, A. G., & Elitzur, M. 1989, ApJ, 346, 991
- Kawabata, K. S., Ohya, Y., Ebizuka, N., Takata, T., Yoshida, M., Isogai, M., Norimoto, Y., Okazaki, A., & Saitou, M. S. 2006, AJ, 132, 433
- Kellogg, E., Pedelty, J. A., & Lyon, R. G. 2001, ApJ, 563, L151
- Kenyon, S. J. 1986, The Symbiotic Stars, Cambridge: Cambridge University Press

- Lane, B.F. et al. 2007, *ApJ*, 658, 520
- Lloyd, H. M., Bode, M. F., O’Brien, T. J., & Kahn, F. D. 1993, *MNRAS*, 265, 457
- Lynch, D. K. et al. 2006, *ApJ*, 638, 987
- MacFadyen, A.I. & Woosley, S.E. 1999, *ApJ*, 524, 262
- Mioduszewski, A.J. & Rupen, M.P. 2004, *ApJ*, 615, 432
- Munrai, U. & Zwitter, T. 2002, *A&A*, 383, 188
- Monnier, J.D. et al. 2006, *ApJ*, 647, L127
- Narumi, H., Hirosawa, K., Kanai, K., Renz, W., Pereira, A., Nakano, S., Nakamura, Y., & Pojmanski, G. 2006, *IAU Circ.*, 8671
- Ness, J.-U., et al. 2006, *IAU Circ.*, 8683
- Nichols, J. et al. 2007, *ApJ*, 660, 651
- O’Brien, T. J., Bode, M. F., & Kahn, F. D. 1992, *MNRAS*, 255, 683
- O’Brien, T. J., Muxlow, T. W. B., Garrington, S. T., Davis, R. J., Eyres, S. P. S., Bode, M. F., Porcas, R. W., & Evans, A. 2006, *IAU Circ.*, 8684
- O’Brien, T. J., Muxlow, T. W. B., Garrington, S. T., Davis, R. J., Porcas, R. W., Bode, M. F., Eyres, S. P. S., & Evans, A. 2006, *IAU Circ.*, 8688
- O’Brien, T. J., Bode, M. F., Porcas, R. W., Muxlow, T. W. B., Eyres, S. P. S., Beswick, R. J., Garrington, S. T., Davis, R. J., & Evans, A. 2006, *Nature*, 443, 279
- Osborne, J., et al. 2006a, *The Astronomer’s Telegram*, 764
- Osborne, J., et al. 2006b, *The Astronomer’s Telegram*, 770
- Padin, S., Davis, R. J., & Bode, M. F. 1985, *Nature*, 315, 306
- Pojmanski, G. 2006, *IAU Circ.*, 8671
- Pooley, G. G., Sokoloski, J. L., Rupen, M. P., & Mioduszewski, A. J. 2006, *The Astronomer’s Telegram*, 750
- Porcas, R. W., Davis, R. J., & Graham, D. A. 1987, in *RS Ophiuchi (1985) and the Recurrent Nova Phenomenon* (ed. M.F. Bode), Utrecht: VNU Science Press, 187

- Quiroga, C., Brandi, E., Ferrer, O. E., García, L. G., & Mikolajewska, J. 2003, BAAA, 46, 35
- Roeser, S. & Bastian, U. 1988, A&AS, 74, 449
- Seaquist, E. R. 1989, in *Classical Novae* (eds. M. F. Bode & A. Evans), Chichester: Wiley, 143
- Sokoloski, J. L., Kenyon, S. J., Brocksopp, C., Kaiser, C. R., & Kellogg, E.M. 2004, in *Revista Mexicana de Astronomia y Astrofisica Conference Series v. 20* (eds. G. Tovmassian & E. Sion), 35
- Sokoloski, J. L., Luna, G. J. M., & Mukai, K. 2006, *The Astronomer's Telegram*, 747
- Sokoloski, J. L., Luna, G. J. M., & Mukai, K. 2006, *The Astronomer's Telegram*, 754
- Sokoloski, J. L., Luna, G. J. M., & Mukai, K. 2006, *The Astronomer's Telegram*, 741
- Sokoloski, J. L., Mukai, K., & Luna, G. J. M. 2006, *The Astronomer's Telegram*, 737
- Sokoloski, J.L., Luna, G.J.M., Mukai, K., & Kenyon, S.J. 2006, *Nature*, 442, 276
- Sostero, G., & Guido, E. 2006, *IAU Circ.*, 8673
- Sostero, G., & Guido, E. 2006, *IAU Circ.*, 8681
- Spoelstra, T. A. T., Taylor, A. R., Pooley, G. G., Evans, A., & Albinson, J. S. 1987, *MNRAS*, 224, 791
- Tatischeff, V. & Hernanz, M. 2007, *ApJ*, 663, L101
- Taylor, A. R., Davis, R. J., Porcas, R. W., & Bode, M. F. 1989, *MNRAS*, 237, 81
- Waagen, E., Labordena, C., Pearce, A., Granslo, B., Otten, C., Mavrofridis, G., & Muylaert, E. 2006, *IAU Circ.*, 8688
- Wallerstein, G. 1958, *PASP*, 70, 537
- Weiler, K.W., Panigia, N., Montes, M.J., & Sramek, R.A. 2002, *ARA&A*, 40, 387
- West, J. D. 2006, *IAU Circ.*, 8683
- Zacharias, N., Monet, D., Levine, S., Urban, S., Gaume, R., & Wycoff, G. 2004, *BAAS*, 205, 4815